ELSEVIER

1 December 1998

OPTICS COMMUNICATIONS

Optics Communications 157 (1998) 115–120

Wavelet analysis of low frequency fluctuations of a semiconductor laser

C. Masoller [a,d], A. Figliola [b], M. Giudici [b], J.R. Tredicce [c], N.B. Abraham [d]

[a] *Instituto de Física, Facultad de Ciencias, Universidad de la República, Montevideo, Uruguay*
[b] *Instituto de Cálculo, FCEN, UBA, Buenos Aires, Argentina*
[c] *Institut Non Lineaire de Nice, Université de Nice-Sophia-Antipolis, CNRS UMR, 06560 Valbonne, France*
[d] *Department of Physics, Bryn Mawr College, 101 N. Merion Ave., Bryn Mawr, PA 19010-2899, USA*

Received 6 March 1998; revised 4 September 1998; accepted 9 September 1998

Abstract

Wavelet transform analysis of experimentally measured intensity fluctuations distinguishes the transition from low frequency fluctuations at moderate feedback to stable operation at strong feedback. Comparison of these results with those of a wavelet analysis of lowpass filtered solutions of the Lang-Kobayashi equations for deterministic evolution of a single mode semiconductor laser with optical feedback finds substantial agreement in the part of the wavelet spectrum corresponding to slow dynamics. Substantial disagreement is found in the fast dynamics, which lessens when noise is added to the equations.

PACS: 42.55.Px; 05.45.+b; 42.65.Sf

Semiconductor lasers with optical feedback have been extensively studied in recent years. It is well known that the linewidth of a single-mode laser diode can be reduced considerably with optical feedback [1], but optical feedback may also excite many external cavity modes and induce chaotic behavior [2,3].

When the laser is operated well above its solitary laser threshold, moderately strong feedback induces what has been termed coherence collapse [4], which is characterized by apparently random intensity fluctuations and a broad band spectrum. When the laser is operated near threshold, moderate feedback induces what has been termed low frequency fluctuations (LFFs), which consist of abrupt intensity drop-outs followed by gradual, stepwise, recoveries (see the first column of Fig. 1). These intensity fluctuations lead to a broad feature at low frequencies in the spectrum. For very strong feedback levels the power drop-outs are suppressed and stable operation is achieved (Regime V of the Tkach-Chraplyvy classification [5]).

The dynamics of a single-longitudinal mode laser diode with optical feedback has been often described by the Lang-Kobayashi (LK) model [6]. The model consists of rate equations for the complex electric field, E, and for the carrier density, N. The external cavity is described by two parameters: the feedback strength, γ, and the round-trip time in the external cavity, τ. A term proportional to $\gamma E(t-\tau)$ accounts for the field reflected from the external mirror. In spite of the limitations of the model (it considers only a single longitudinal mode of the solitary laser, and a single reflection in the external cavity), it reproduces the observed behavior remarkably well over a wide range of parameter values [2,3].

The phenomenon of low frequency fluctuations has been studied theoretically and experimentally by several groups [7–17]. The LFFs are actually a slow envelope modulation of a series of fast intensity pulses [12] (of the order of picosecond pulse widths), and simulations based on the LK model [7,10,12] and on a travelling-wave model [13] have shown similar fast pulses. After time averaging the output power fluctuations of the numerical solutions (to simulate the bandwidth of the detectors used in most experiments), power drop-outs are also found.

0030-4018/98/$ - see front matter
PII: S0030-4018(98)00489-1

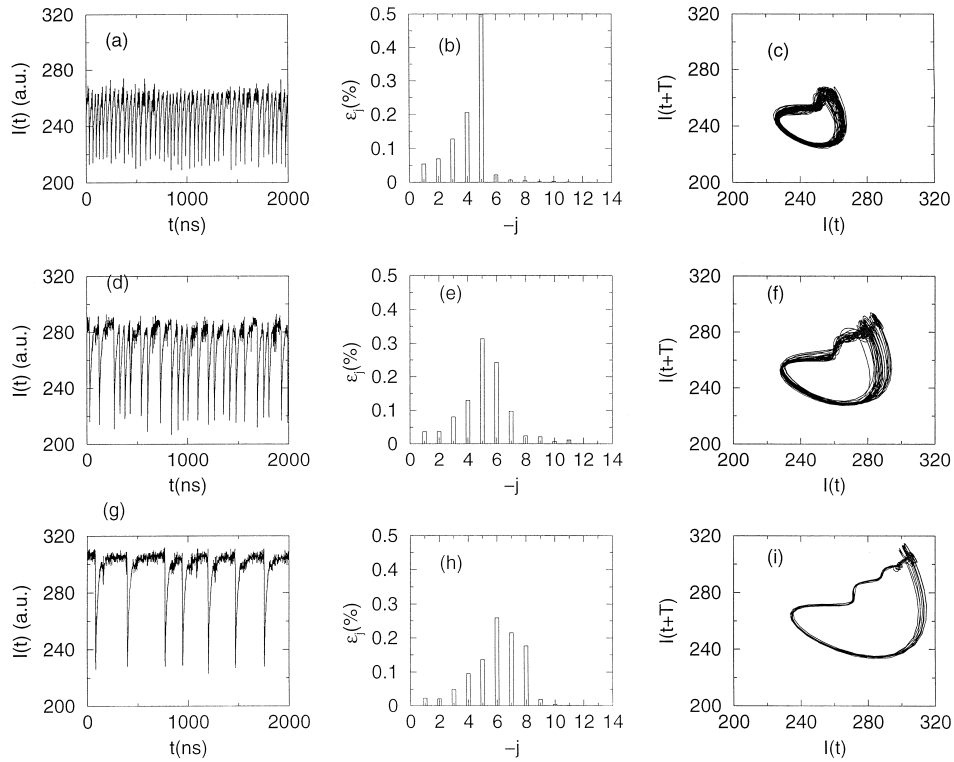

Fig. 1. Measured time dependence of the output power for increasing feedback (2000 data points are shown). The voltage in the acousto-optic modulator is (a) 400 mV, (d) 300 mV, (g) 200 mV. Energy distribution among the wavelet bands for (b) $V = 400$ mV, (e) $V = 300$ mV, (h) $V = 200$ mV. Reconstruction of the attractor (500 data points are shown). $T = 7\Delta t$. (c) $V = 400$ mV, (f) $V = 300$ mV, (i) $V = 200$ mV.

In spite of the successful simulations, there is still an ongoing debate on the physical origin of the LFFs. Recent experimental measurements by Huyet et al. show that the probability distribution of the intensity fluctuations during the drop-outs is strongly asymmetric and peaks at about the average intensity [15], indicating the presence of fluctuations from zero intensity to two or three times the average intensity. This differs from simulations based on the LK model, where the laser is switched off most of the time (between the short pulses) and thus the intensity probability distribution in this case is peaked at zero and decreases continuously. Moreover, time resolved optical spectra reveal that the emergence of LFFs is associated with the excitation of several longitudinal modes; during the power drop-outs they are synchronized and drop out together [16,17].

In this report we use the discrete wavelet transform (DWT) to analyze the intensity fluctuations in the LFF regime. The wavelet transform is particularly useful in the study of non-stationary signals. It represents a signal in terms of brief waveforms (a wavelet is a smooth and rapidly vanishing oscillating function with a good localization both in frequency and in time), and therefore the wavelet transform is suitable to study singularities such as transients or short pulses.

Two of us have previously used the DWT to analyze numerical simulations (based on the LK model) of the transient dynamics from stable operation to the coherence collapsed regime [18]. It was shown that with the wavelet transform the jumps among destabilized external cavity modes could be easily distinguished, because they lead to brusque variations in the energy distribution among the wavelet bands in the phase delay signal. (These jumps could not be detected in the wavelet transform of the intensity signal, because in the intensity signal the energy is concentrated mainly in the wavelet band contaning the relaxation oscillation frequency of the solitary laser.)

Here we use the DWT to analyze experimentally measured intensity signals, and time-averaged (low-pass filtered) solutions of the LK model, in the LFF regime.

A wavelet family $\psi_{a,b}$ is a set of functions generated by dilations and translations of a mother wavelet $\psi(t)$ [19–21],

$$\psi_{a,b}(t) = |a|^{-1/2}\psi\left(\frac{t-b}{a}\right), \tag{1}$$

where a, $b \in \mathbb{R}$ are the scale and translation parameters

respectively, and t is the time. As a increases, the mother wavelet becames narrower, and thus we have a unique analytic pattern and its replicas at different scales with variable localization in time. The DWT is obtained for special selections of the mother wavelet, and a discrete set of parameters

$$a_j = 2^{-j} \quad \text{and} \quad b_{j,k} = 2^{-j}k, \tag{2}$$

with $j,\ k \in \mathbb{Z}$. The DWT of a signal $x(t)$ is the set of coefficients $c_{j,k}$, called wavelet coefficients, which are obtained by the decomposition of $x(t)$ onto the basis of functions $\psi_{j,k}$,

$$c_{j,k} = \langle x(t), \psi_{j,k}(t) \rangle, \tag{3}$$

where

$$\psi_{j,k}(t) = 2^{j/2}\psi(2^j t - k). \tag{4}$$

We have chosen a cubic spline wavelet basis and used the pyramidal algorithm to compute nearly 2^{-j} wavelet coefficients for each $j = -1, \ldots, -|\log N|$. The DWT breaks down a signal into successive logarithmically spaced frequency bands. The experimentally measured intensity signals consist of 10000 data points sampled with $\Delta t = 1$ ns. The DWT decomposes the signal into 13 wavelet bands, the wavelet band $-j = 1$ represents the frequency band 0.25–0.5 GHz; $-j = 2$: 0.125–0.25 GHz, $-j = 3$: 0.062–0.125 GHz, $-j = 4$: 0.031–0.062 GHz, $-j = 5$: 0.015–0.031 GHz, etc.

Since the wavelet basis is orthonormal,

$$\langle x(t)^2 \rangle \propto \sum_j \sum_k |c_{j,k}|^2, \tag{5}$$

and the energy associated with level j (or scalogram) is

$$\epsilon_j = \sum_k |c_{j,k}|^2. \tag{6}$$

For the experiments the laser (Hitachi HLP 1400 emitting at 830 nm) was biased 5% above the solitary laser threshold, $I_{th} = 81$ mA, and the feedback was varied with an acousto-optic modulator. The laser intensity as a function of time was measured with a fast photodiode. The experimental setup is described in detail in Ref. [17].

The first column of Fig. 1 shows the intensity fluctuations for three different values of the voltage, V, in the acousto-optic modulator. (The levels in the y-axis on the first column of Fig. 1 are arbitrary, and because of the ac-coupled data-adquisition system, the zero level is unknown.) Also note that the larger the value of V, the lower the feedback level.

The intensity shows abrupt drop-outs followed by gradual, stepwise recoveries. For moderate feedback the drop-outs are nearly periodic, and the average time between consecutive drop-outs is about 40 ns (Fig. 1(a)). The length of the steps in the build-up phase after the power drop-out is about 3 ns. For greater feedback the drop-outs become less frequent, and the laser reaches stable operation for sufficiently high feedback. At all feedback values the duration of the build-up phase is about 10 steps.

The energy distribution among the wavelet bands is shown in the second column of Fig. 1. For moderate feedback the energy is carried by the bands $-j \leq -5$, with approximately half of the energy carried by the band $-j = 5$ (Fig. 1(b)). This band contains the mean frequency of the drop-outs. The low frequency bands ($-j \geq 6$) carry very little energy. For higher feedback the drop-outs are less frequent, there is not a well defined average time between drop-outs, and the energy is distributed among a larger number of wavelet bands (mainly in the bands $-j = 6$, $-j = 7$, and $-j = 8$).

By sliding a 128 data set window along the time series we studied the time evolution of the energy distribution. The energy in all wavelet bands increases in the time intervals which contain a power drop-out. In these intervals, the bands $-j = 5$ and $-j = 6$ carry the major part of the energy. In the other time intervals, the bands $-j = 1$ and $-j = 2$ are the ones that carry more energy (they contain the frequencies of the fast oscillations in between power drop-outs).

In order to investigate in more detail the stabilization process for increasing feedback we developed a filter based on the wavelet transformation and obtained a 'cleaner' intensity signal.

With the DWT a signal can be decomposed in smother versions, plus the details that take into account the high frequencies corresponding to each level. In other words, at level j a residual signal can be obtained, which is a smoothed version with less high frequencies than the previous level $j + 1$ ($j < 0$) [22,23]. The residual signal has half the data of the previous level, and an interpolation with spline functions was used to obtain the remaining data [24]. This method allows the elimination of frequency bands not desired that mask interesting phenomena. Due to the orthogonality of the wavelet functions employed, the filter extracts the desired frequency bands without distorting the retained bands. We filtered out the bands $-j = 1$ and $-j = 2$, thereby discarding many of the fast oscillations that occur in between the power drop-outs. As an example, Fig. 2(a) shows the filtered intensity signal corresponding to a voltage $V = 300$ mV in the acousto-optic modulator (the solid line in Fig. 2(a) indicates the filtered signal and the dashed line, the experimentally measured signal).

We reconstructed the underlying attractor applying the time delay method. The results, shown in the third column of Fig. 1, suggest a behavior which is typical of intermittency. We have only shown the first 500 data points (corresponding to the first 500 ns of evolution) to make the plot readable. It is clear that the attractor has a 'tunnel' which becomes narrow for increasing feedback. This might be the reason why the drop-outs become less frequent for increasing feedback. When the trajectory arrives near the entrance of the tunnel, a drop-out occurs. Our results are

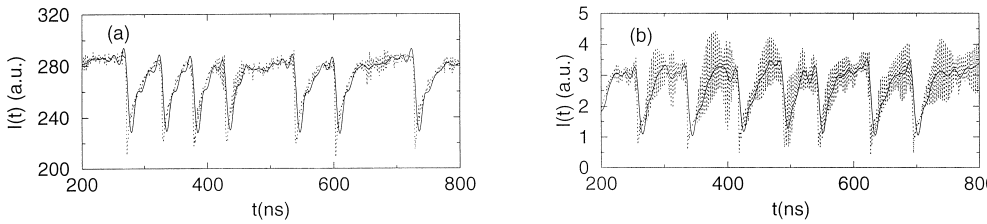

Fig. 2. (a) Experimentally measured intensity signal for $V = 300$ (dashed line) and filtered signal (solid line). (b) Numerically simulated intensity signal for $\gamma = 150$ GHz (dashed line) and filtered signal (solid line).

consistent with the interpretation of Refs. [15,16] that noise induces the drop-outs and that the laser recovers in a deterministic fashion.

For comparison, we have numerically solved the deterministic LK model. The LK equations are

$$\frac{dE}{dt} = \frac{1 + i\alpha}{2}\left(G - \frac{1}{\tau_p}\right)E + \gamma E(t-\tau)e^{-i\omega_0\tau}, \qquad (7)$$

$$\frac{dN}{dt} = J - \frac{N}{\tau_s} - G|E|^2. \qquad (8)$$

In these equations the slowly varying complex electric field is normalized such that $V|E|^2$ is the total photon number in the laser waveguide, where V is the volume of the active region. τ_s is the carrier lifetime, and τ_p is the photon lifetime. ω_0 is the solitary laser frequency. The optical gain is $G = G_N(N - N_0)/(1 + \epsilon|E|^2)$, where G_N is the modal gain, N_0 the carrier density at transparency, and ϵ the gain saturation coefficient. α is the linewidth enhancement factor, and J is the current density in carriers per unit volume and unit time. The equations were integrated with a fourth-order Runge-Kutta method, and the parameters were chosen to keep our simulations close to the experiments. The parameters are: $\tau_s = 1$ ns, $\tau_p = 1.4$ ps, $\tau = 3$ ns. $\omega_0\tau = 6$ rad, $G_N = 1.06 \times 10^{-12}\ m^3\ s^{-1}$, $N_0 = 3.55 \times 10^{24}\ m^{-3}$, $\epsilon = 2 \times 10^{-24}\ m^3$, $\alpha = 4.5$, $V = 1.2 \times 10^{-16}\ m^3$, and $J = 1.05J_{th}$, where J_{th} is the threshold current density ($J_{th} = N_{th}/\tau_s$, where N_{th} is the threshold carrier density, which satisfies $G_N(N_{th} - N_0) = 1/\tau_p$). For these parameters, the threshold current $I_{th} = eVJ_{th}$ (where e is the electron charge) is 81 mA, and the relaxation oscillation frequency of the solitary laser is about 2 GHz.

The numerically simulated intensity signal shows fast, picosecond pulses, as has been found previously in the literature [10,12]. To make comparisons with the experiments, the finite bandwidth of the detectors used in the experiments must be taken into account. Since in the experiments the intensity was measured with a 6 GHz bandwidth detector [17], we averaged the simulated fast pulsing intensity over 1 ns. The first column of Fig. 3. shows the results obtained for three different feedback levels.

The time-averaged intensity exhibits irregular drop-outs and subsequent recoveries that are similar to those observed in the experiments. However, there are important quantitative deviations. The steps in the build-up phase after a drop-out, and the fast oscillations that occur in between two consecutive drop-outs are much more pronounced in the calculated time-averaged intensity than in the experimentally measured intensity. Moreover, the mean value of the experimentally measured intensity is rougly constant before a drop-out, while the mean value of the simulated time-averaged intensity shows important fluctuations, indicating that in the simulated signal, when a drop-out occurs the intensity did not totally recover of the previous drop-out.

The energy distribution among the wavelet bands for each feedback level is shown in the second column of Fig. 3. Comparing with the second column of Fig. 1 it is clear that the results obtained from the simulated time-averaged intensity are similar to those obtained from the experimental data. However, at all feedback levels the energy in the first wavelet band is much larger in the simulated data than in the experimental data.

To make more precise comparisons, we filtered out the first two wavelet bands of the numerically simulated time-averaged intensity. In Fig. 2(b) we show the results for a feedback level $\gamma = 150$ GHz. The solid line indicates the filtered signal, and the dashed line indicates the original signal. The underlying attractors, reconstructed by the time-delay method, are shown in the third column of Fig. 3. To make the features of the attractor more clear, only the first 500 data points are shown.

The size of the attractor grows with the feedback level (as occurs with the size of the attractor reconstructed from the experimental signal). However, while the tunel in the 'experimental' attractor becomes narrower with the feedback, the tunel in the 'simulated' attractor grows together with the attractor size.

This is related with the fact that the way the stable operation regime is reached for increasing feedback in the LK model differs from that in the experiments. In the numerical simulations the stable regime is reached after a long LFF transient that becomes shorter with increasing feedback. This is explained by the fast dynamics underly-

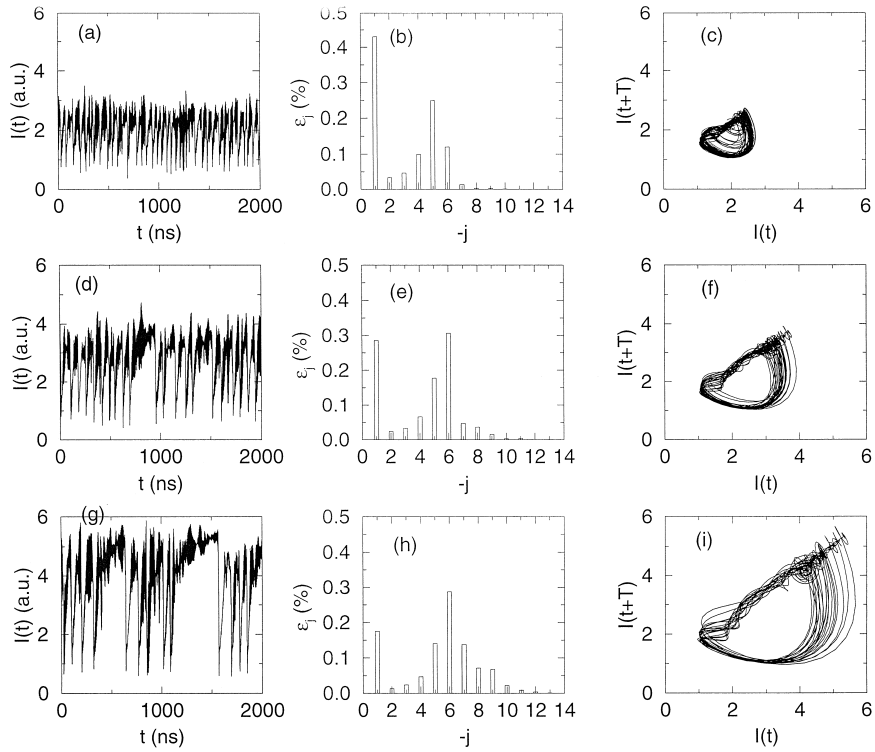

Fig. 3. Results of the numerical simulation of the LK equations (2000 data points are shown). The intensity was averaged over 1 ns (a) $\gamma = 110$ GHz, (d) $\gamma = 150$ GHz, (g) $\gamma = 190$ GHz. Energy distribution among the wavelet bands for (b) $\gamma = 110$ GHz, (e) $\gamma = 150$ GHz, (h) $\gamma = 190$ GHz. Reconstruction of the attractor (500 data points are shown). $T = 7\Delta t$. (c) $\gamma = 110$ GHz, (f) $\gamma = 150$ GHz, (i) $\gamma = 190$ GHz.

ing the LFFs. For moderate feedback the laser jumps among a large number of destabilized external cavity modes [7,10,12]. The oscillations become larger for increasing feedback, and eventually the laser reaches the external cavity mode with lowest threshold gain (or one of its neighbors), which are stable as shown by Levine et al.

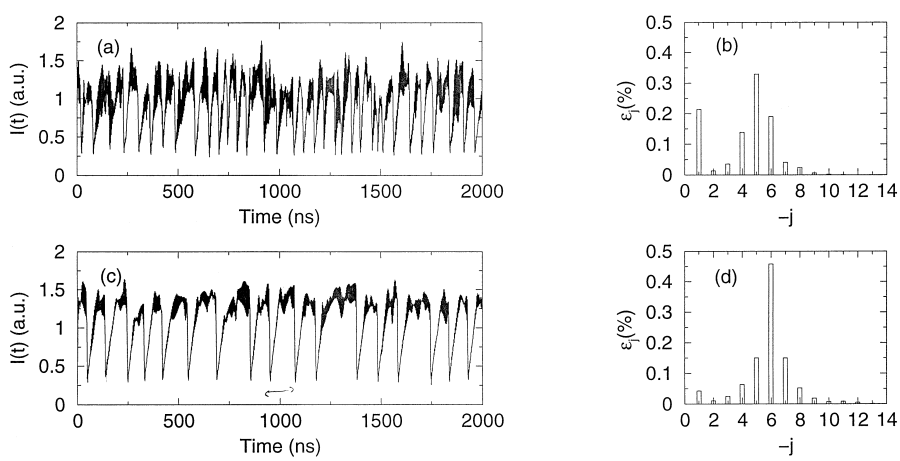

Fig. 4. (a), (b) Results of the deterministic LK equations. $\gamma = 100$ GHz. (c), (d) Results of the stochastic LK equations. $\gamma = 100$ GHz, and the noise strengh is 50 GHz.

[25]. Then, the laser remains in this stable state (which persists over a certain feedback range if we slowly decrease the feedback level). Moreover, this state is stable when moderate noise levels are included in the rate equations [26]. However, in the experiments the drop-outs gradually become less frequent for increasing feedback, until they disappear.

To check whether the discrepancies found might be related to the absence of spontaneous emission noise in the simulations, we included in the field rate equation a Langevin noise term of strength comparable to the feedback term. Figs. 4(a), 4(b) [Figs. 4(c), 4(d)] can be used to compare the results obtained from the deterministic and stochastic models. Clearly the inclusion of noise leads to a better agreement between the numerical simulations and the experiments. Noise makes the drop-outs less frequent, and the time-averaged intensity less noisy. (Hohl et al. [11] have shown that in certain parameter regions the inclusion of noise has important effects on the statistical distribution of the drop-outs.) However, the fast oscillations are still more important in the time-averaged intensity obtained from simulation of the stochastic model than in the experimental intensity, and while the energy distribution among the wavelet bands in the first case is concentrated in the wavelet band $-j = 6$ (Fig. 4(d)), in the experimental intensity it is distributed among a larger number of wavelet bands (see, e.g., Fig. 1(h)).

In conclusion, we find that the discrete wavelet transform gives more compact information about LFFs, and after filtering it gives a better reconstruction of the measured dynamics than does Fourier analysis. The advantage of the wavelet method over traditional filtering is that removing certain frequency bands does not modify the dynamics relying on the remaining bands. The key of this success is that wavelets are localized oscillations which do not have the correlations of sine waves over extended time. The wavelet transform can separate the amplitudes of the fast and slow components (in the wave-packet bases) of a signal, and can be used to reconstruct the signal (by wavelet transforming, selecting only some of the wavelet amplitudes, and then inverse transforming and interpolating).

Our results show that the experimental intensity signal looks more like a 'wavelet-transform filtered' simulated intensity than a simple averaging of the simulated intensity. The wavelet analysis shows that the difference between the experimental data and the simulations based in the LK model is in the 'fast and short' components of the signal. This suggests that the LK model is useful for a qualitative description of LFFs (since it describes the average features of LFFs in good agreement with experiments), but quantitative differences remain which need further explanation. We speculate that the Lang-Kobayashi equations are too 'stiff', and a more accurate model will have to have additional field and/or population variables whose dissipation softens the impulse response of the LK equations to abrupt changes.

Acknowledgements

We wish to acknowledge useful discussions with G. Mindlin. This research work was partially supported by the PEDECIBA (Uruguay), and the CONICET (Argentina).

References

[1] G.P. Agrawal, N.K. Dutta, Long-Wavelength Semiconductor Lasers, Van Nostrand Reinhold, New York, 1986
[2] K. Petermann, IEEE J. Sel. Top. Quantum Electron. 1 (1995) 480.
[3] G.H.M. van Tartwijk, D. Lenstra, Quantum Semiclass. Opt. 7 (1995) 87.
[4] D. Lenstra, B.H. Verbeck, A.J. den Boef, IEEE J. Quantum Electron. 21 (1985) 674.
[5] R.W. Tkach, A.R. Chraplyvy, IEEE J. Lightwave Technol. 4 (1986) 1655.
[6] R. Lang, K. Kobayashi, IEEE J. Quantum Electron. 16 (1980) 347.
[7] T. Sano, Phys. Rev. A 50 (1994) 2719.
[8] P. Besnard, B. Meziane, K. Ait-Ameur, G. Stephan, IEEE J. Quantum Electron. 30 (1994) 1713.
[9] E. Cerboneschi, F. de Tomasi, E. Arimondo, IEEE J. Quantum Electron. 30 (1994) 2277.
[10] G.H.M. van Tartwijk, A.M. Levine, D. Lenstra, IEEE J. Sel. Topics Quantum Electron. 1 (1995) 466.
[11] A. Hohl, H.J.C. van der Linden, R. Roy, Optics Lett. 20 (1995) 2396.
[12] I. Fischer, G.H.M. van Tartwijk, A.M. Levine, W. Elsasser, E. Gobel, D. Lenstra, Phys. Rev. Lett. 76 (1996) 220.
[13] P.S. Spencer, K.A. Shore, Quantum Semiclass. Opt. 9 (1997) 819.
[14] B. Tromborg, J. Mork, V. Velichansky, Quantum Semiclass. Opt. 9 (1997) 831.
[15] G. Huyet, S. Hegarty, M. Giudici, B. de Bruyn, J.G. McInerney, Europhys. Lett. 40 (1997) 619.
[16] M. Giudici, C. Green, G. Giacomelli, U. Nespolo, J.R. Tredicce, Phys. Rev. E 55 (1997) 6414.
[17] G. Huyet, S. Balle, M. Giudici, C. Green, G. Giacomelli, J.R. Tredicce, Optics Comm. 149 (1998) 341.
[18] A. Figliola, C. Masoller, Phys. Rev. A 56 (1997) 1492.
[19] I. Daubechies, Ten Lectures on Wavelets, SIAM, Philadelphia, 1992.
[20] Y. Meyer, Wavelet Alghoritms and Applications, SIAM, Philadelphia, 1992.
[21] C. Chui, An Introduction to Wavelets, Academic Press, San Diego, 1992.
[22] R.R. Coifman, Adapted Multiresolution Analysis, Computation, Signal Processing and Operator Theory, Proc. International Congress of Mathematicians, Kyoto, Japan, Springer-Verlag, 1990, pp. 879–887.
[23] S. Blanco, A. Figliola, R. Quian Quiroga, O.A. Rosso, E. Serrano, Phys. Rev. E 57 (1998) 932.
[24] I.J. Schoenberg, Cardinal spline interpolation, SIAM, Philadelphia, 1993.
[25] A.M. Levine, G.H.M. van Tartwijk, D. Lenstra, T. Erneux, Phys. Rev. A 52 (1995) R3436.
[26] J. Wieland, C.R. Mirasso, D. Lenstra, Optics Lett. 22 (1997) 469.